Analyst

PAPER

Cite this: *Analyst*, 2015, **140**, 736

High finesse optical cavity coupled with a quartz-enhanced photoacoustic spectroscopic sensor

Pietro Patimisco,[a] Simone Borri,[b] Iacopo Galli,[b] Davide Mazzotti,[b] Giovanni Giusfredi,[b] Naota Akikusa,[c] Masamichi Yamanishi,[d] Gaetano Scamarcio,[a] Paolo De Natale[b] and Vincenzo Spagnolo*[a]

An ultra-sensitive and selective quartz-enhanced photoacoustic spectroscopy (QEPAS) combined with a high-finesse cavity sensor platform is proposed as a novel method for trace gas sensing. We call this technique Intra-cavity QEPAS (I-QEPAS). In the proposed scheme, a single-mode continuous wave quantum cascade laser (QCL) is coupled into a bow-tie optical cavity. The cavity is locked to the QCL emission frequency by means of a feedback-locking loop that acts directly on a piezoelectric actuator mounted behind one of the cavity mirrors. A power enhancement factor of ~240 was achieved, corresponding to an intracavity power of ~0.72 W. CO_2 was selected as the target gas to validate our sensor. For the P(42) CO_2 absorption line, located at 2311.105 cm^{-1}, a minimum detection limit of 300 parts per trillion by volume at a total gas pressure of 50 mbar was achieved with a 20 s integration time. This corresponds to a normalized noise equivalent absorption of 3.2×10^{-10} W cm^{-1} $Hz^{-1/2}$, comparable with the best results reported for the QEPAS technique on much faster relaxing gases. A comparison with standard QEPAS performed under the same experimental conditions confirms that the I-QEPAS sensitivity scales with the intracavity laser power enhancement factor.

Received 27th June 2014
Accepted 24th November 2014

DOI: 10.1039/c4an01158a

www.rsc.org/analyst

Introduction

High resolution and high sensitivity spectroscopic techniques incorporating laser sources are key tools in gas monitoring and trace detection applications. They are nonintrusive, do not require sample preparation, provide real-time information and allow *in situ* monitoring or remote detection.[1,2] By using mid-infrared (IR) laser sources it is possible to get access to strong fundamental vibrational bands, located in the molecular fingerprint spectral region between 4 μm and 12 μm, of a large number of gas molecules of fundamental and/or applied interest, allowing highly sensitive and selective detections. Quantum cascade lasers (QCLs) provide complete coverage of this wide spectral region, and have been demonstrated to be suitable for a large variety of spectroscopic techniques including frequency-modulation spectroscopy,[3] cavity-enhanced absorption spectroscopy[4] (CEAS), cavity ring-down spectroscopy[5] (CRDS), photoacoustic spectroscopy[6] (PAS), and quartz-enhanced PAS[7] (QEPAS). The commercial availability of room temperature continuous-wave external cavity QCLs with wide tuning ranges (up to 200 cm^{-1}), high power and relatively narrow linewidth[8] enables both multi-component sensing and detection of broadband molecular absorbers.

Photoacoustic spectroscopy (PAS) is one of the most used spectroscopic techniques for trace gas sensing applications due to its high sensitivity and selectivity.[6] Energy deposited in the gas of interest *via* absorption of modulated optical radiation is converted to local heating by collisional processes, thereby creating a pressure wave (sound) in an acoustic cell. The photoacoustic signal is detected by sensitive microphones and its strength can be enhanced by modulating the excitation source at a frequency matching an acoustic resonance of the cell. A well-established variation of the conventional PAS is the QEPAS technique that was first reported in 2002.[9] This technique uses a mm-size piezoelectric quartz tuning fork (QTF) as an acoustic wave transducer operating in quadrupole mode. This, together with the high *Q*-factor and the ~32.7 kHz resonance frequency of the QTF, provides immunity to environmental acoustic noise. Moreover, QEPAS has demonstrated a large dynamic range of up to nine orders of magnitude of the photoacoustic signal and its noise is ultimately limited by the fundamental Johnson thermal noise of the QTF.[10] Different QEPAS configurations have been demonstrated, such as on-beam,[9,10] off-beam,[11] modulation cancellation[12] and evanescent wave QEPAS.[13] Very recently, QEPAS combined with mid-IR QCL sources has demonstrated record sensitivities up to 50 parts-per-trillion (ppt) concentration levels in 1 s lock-in time constant for SF_6

[a]*CNR-IFN UOS Bari and Dipartimento Interateneo di Fisica, Università e Politecnico di Bari, via Amendola 173, 70126 Bari, Italy. E-mail: vincenzoluigi.spagnolo@poliba.it*
[b]*CNR-INO UOS Sesto Fiorentino and LENS, via Carrara 1, 50019 Sesto Fiorentino FI, Italy*
[c]*Development Bureau Laser Device R&D Group, Hamamatsu Photonics KK, Shizuoka 434-8601, Japan*
[d]*Central Research Laboratories, Hamamatsu Photonics KK, Shizuoka 434-8601, Japan*

detection.[14,15] The intensity of the QEPAS signal is directly proportional to the power absorbed by the target species and thus the sensitivity varies linearly with the laser power. Up to 1 W of optical power has been used for QEPAS sensing.[16] One alternative way to increase the laser power can be the employment of power build-up approaches, like the one occurring in high-finesse optical cavities.

Very recently, we reported on the first realization of a novel spectroscopic technique combining QEPAS with CEAS, which we call intra-cavity QEPAS (I-QEPAS),[17] demonstrating CO_2 detection sensitivities in the parts per trillion (ppt) concentration range. Also, in ref. 17 is reported an exhaustive comparison with already published optical sensors, in terms of CO_2 trace detection. We will report here a detailed description of the design and characterization of this innovative technique and its comparison with a standard QEPAS sensor operating under the same experimental conditions. We will also provide a detailed discussion about the characteristics of the compact bow-tie four-mirror optical resonator developed for the I-QEPAS apparatus and the locking loop performances.

Experimental set-up

Within an optical cavity, light is reflected repeatedly by high-reflectivity mirrors, giving rise to a power enhancement proportional to the number of round-trips (enhancement factor) in correspondence to well defined frequency values (cavity resonance frequencies). The resonance frequencies occur every c/L, where c is the speed of light and L the round-trip length and the spectral separation between two consecutive resonances is the so-called free-spectral range (FSR). The quality of an optical resonator strongly depends on the cavity losses (including residual transmission or absorption by the mirrors) and it is measured by a parameter called finesse (F), which is defined as the ratio between the FSR and the resonance full-width at half maximum value $\Delta\nu$: $F = \mathrm{FSR}/\Delta\nu$. The finesse can also be calculated by taking into account the total cavity losses per round trip, $1 - \rho$, according to $F = 2\pi/(1 - \rho)$. For ring cavities, a power enhancement factor E up to F/π can be obtained for perfect mode and impedance matching.[4] As a consequence, the higher the finesse (*i.e.* the mirror reflectivity), the larger is the power enhancement factor and the narrower is the resonance width. With mirror reflectivities > 99%, the cavity will easily have a series of evenly spaced, sharp resonances with linewidths even smaller than 10 MHz.[18] In CEAS setups, the laser wavelength has to be matched with one of the cavity resonances, and a proper locking between the laser frequency and the cavity resonance has to be implemented for spectral scans. Usually, two approaches are performed: (i) part of the light exiting the cavity is fed back to the laser[19,20] (optical feedback); (ii) the cavity length is adjusted in order to match the laser frequency. By using a closed-locking loop electronic circuit it is possible to force the laser and the cavity to be in resonance by acting on the cavity itself (typically on a piezoelectric actuator moving one of cavity mirrors).[18] In this second approach, modulation techniques can be used to derive an electronic error signal that represents the deviations of the laser frequency from a given cavity mode. In this way, the laser is kept in resonance with the length of the cavity and a very high spectral resolution can be achieved if high reflectivity mirrors are used. Since a high laser power is required for strong QEPAS signals, the use of optical cavities promises to significantly increase the sensitivity of the QEPAS technique according to the effective power enhancement factor. This factor strongly depends on the cavity finesse and on the quality of the mode matching between the laser and the cavity, which can be optimized by properly handling the beam geometry entering the cavity and by using laser radiation with a linewidth comparable to or narrower than the cavity mode. Recently, free-running continuous-wave QCL linewidths of ~1 MHz or below were demonstrated in combination with low-noise stabilized current sources,[21] and linewidths in the kHz range were demonstrated on QCL by frequency locking to sub-Doppler absorption lines[22] or by phase locking to frequency comb referenced radiation.[23] In addition, when the laser mode matching the TEM_{00} cavity mode is realized, an intra-cavity beam with an excellent spatial beam profile can be obtained, which is advantageous for a proper focalization of the beam between the prongs of the quartz tuning fork.[15]

The experimental sensor platform is shown in Fig. 1.

The laser source is a room-temperature continuous-wave distributed-feedback QCL (Hamamatsu Photonics) emitting at 4.33 μm wavelength with a maximum power of 10 mW at 800 mA driving current. The QCL output radiation is collimated by a ZnSe lens (L_1) with a short focal length (20 mm). A polarizing beam splitter transmits part of the laser beam (about 10% in power) towards a reference cell filled with pure CO_2 at about 1 mbar. The beam that exits this cell is collected by a ZnSe lens (L_3) and detected using an HgCdTe liquid-N_2 cooled detector (D_1 in Fig. 1). The beam reflected by the beam splitter is focused into a bow-tie shaped optical cavity composed of 4 mirrors, two spherical mirrors with a radius of curvature of 30 mm (M_1 and M_2 in Fig. 1) and two planes (M_3 and M_4). The total cavity length (round-trip distance) is $L = 174$ mm. The laser beam-cavity optical coupling was realized by employing a CaF_2 plano-convex mode-matching lens (L_2) having a focal length of 100 mm. The coupling between the laser beam and the TEM_{00} optical mode of the cavity was verified by acquiring the laser beam profile

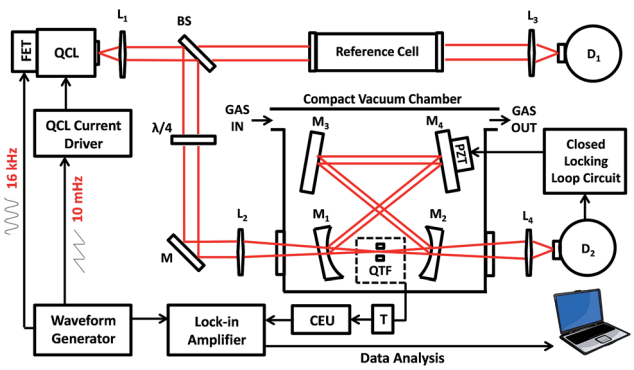

Fig. 1 Schematic of the I-QEPAS apparatus. QCL: quantum cascade laser; FET: field-effect transistor; L: lens; BS: beam-splitter; D: detector; M: mirror; T: transimpedance amplifier; CEU: control electronic unit; QTF: quartz tuning fork.

coming out of the cavity with a pyroelectric camera placed behind M_2. M_4 is connected to a piezoelectric transducer (PZT) which allows a fine tuning of the cavity length up to ~10 μm. All four mirrors use YAG substrates, have a diameter of 0.5 inches and are coated with dielectric layers to reach a reflectivity of R = 99.9% at the laser wavelength and at 10 degrees angle of incidence. The decision of working with tilted mirrors was taken in order to avoid the strong feedback on the QCL induced by the radiation retro-reflected by the input mirror M_1. An InSb infrared detector (D_2 in Fig. 1) is placed after M_2 and collects the radiation exiting the cavity. Its output serves as an error signal for the locking loop between the laser and the cavity. The QTF is mounted on a three-axis translator and is placed between M_1 and M_2. The estimated beam waist ($1/e^2$ radius) between the two spherical mirrors under these operating conditions (neglecting astigmatic distortions) is 60 μm, ensuring a beam diameter well below the spacing between the two prongs of the QTF (~300 μm). The QTF acts as a piezoelectric acoustic transducer able to efficiently detect the pressure wave generated by non-radiative gas relaxation, which follows the laser absorption by the target gas mixture filling the cavity. We experimentally verified that all the intracavity beam power passes between the prongs of the fork without hitting it, which is a mandatory condition in order to reduce thermal noise and spurious background on the photoacoustic signal.[10] The resonator is housed into a vacuum chamber equipped with two anti-reflection coated CaF_2 windows for entrance/exit of the light and filled with the target gas at selected pressures (see Fig. 1). The low-noise current driver is equipped with an input channel allowing for slow (<1 kHz) modulations mode-hop-free frequency tuning of the laser. Faster modulations (up to tens of MHz) can be applied directly to the QCL chip by means of a field-effect transistor (FET). A custom-built control electronics unit (CEU) is used to measure the electrical parameters of the QTF (dynamical resistance R, quality factor Q and resonant frequency f_0). The measured QTF resonance frequency is f_0 = 32 809 Hz, slightly depending on the gas pressure, and the quality factor Q exceeds 30 000 under operative pressure conditions (50 mbar). An electric resistance of 42.1 kΩ was measured, leading to a thermal noise level of 11.6 μV. The piezoelectric signal generated by the QTF was detected by a low noise transimpedance amplifier with a 10 MΩ feedback resistor, converted into a voltage signal and then demodulated by a lock-in amplifier (model EG&G 5210).

Principle of operation of the I-QEPAS technique

The optical properties of the resonator were preliminarily estimated on the basis of the mirror reflectivity according to the equations described in the Experimental section. We calculated a finesse of about 1570 by taking into account only the partial transmittivity of the mirrors as round-trip losses. By measuring the total length of the cavity, the free spectral range results: FSR = c/L = 1.725 GHz. Finally, the cavity mode FWHM can be estimated as the ratio between the FSR and the finesse: $\Delta\nu$ = FSR/F = 1.1 MHz, comparable to the free-running laser linewidth. After alignment, the actual optical properties of the cavity can be precisely measured by recording the signal transmitted by mirror M_2. The operating temperature of the QCL was stabilized at 283 K and the injected current was linearly tuned by applying a slow voltage saw-tooth ramp to the current driver, in order to span an entire FSR. In Fig. 2 a recording of two consecutive transmission peaks (under vacuum conditions) is shown, and a zoom over a single resonance is shown in the inset.

By knowing the FSR, the horizontal scale can be converted into frequency (MHz), and a Lorentzian fit of the cavity mode allows the measurement of its width: $\Delta\nu$ = 1.15 MHz, in good agreement with the estimated value. The measured finesse F of the optical resonator thus results to be F = 1505. In order to calculate the power enhancement factor we have to consider that our cavity does not satisfy the condition for perfect impedance matching (cavity leakage only due to the input and output mirrors, in equal parts), as the internal losses are equally distributed among all the four mirrors. In this case, by calculating the ratio between the intracavity and input field intensities, a power enhancement factor $E = F/2\pi$ = 240 is obtained.

In our experiments, we need to lock the resonance frequency of the cavity to the laser one during the slow linear scan. The simplest way is to adjust accordingly the cavity length by using the PZT *via* an electronic feedback signal. To generate a low noise error signal we add a sinusoidal frequency modulation (at the frequency $f_0/2$) to the laser radiation, so that the signal from the InSb detector demodulated at $f_0/2$ by a lock-in amplifier reproduces the first derivative of the resonator transmission signal, *i.e.* a dispersive error signal centered at zero. An electronic control loop processes the error signal by means of a proportional-integral operational amplifier module and closes the locking loop on the PZT, tuning the cavity length. Robust locking is possible thanks to the laser narrow linewidth and to the low noise error signal obtained on the detector. In Fig. 3 the cavity output in locked mode is shown (black curve), when a

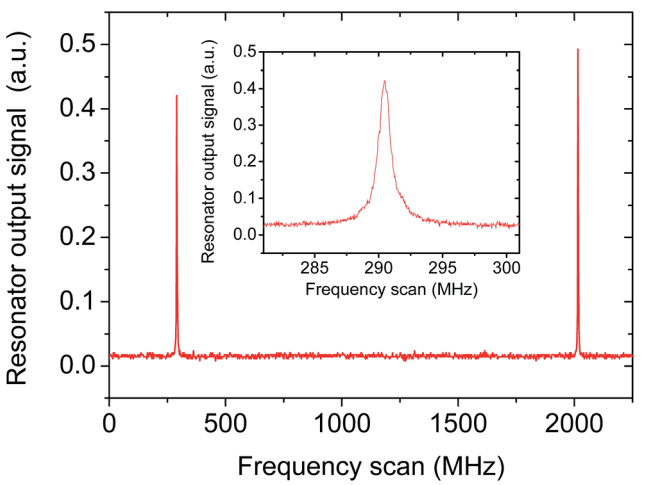

Fig. 2 Cavity transmission spectrum acquired with the liquid-nitrogen cooled InSb detector, when a slow voltage saw-tooth ramp is applied to the QCL current driver and all four mirrors are fixed, under vacuum conditions. Inset: zoom over a cavity mode.

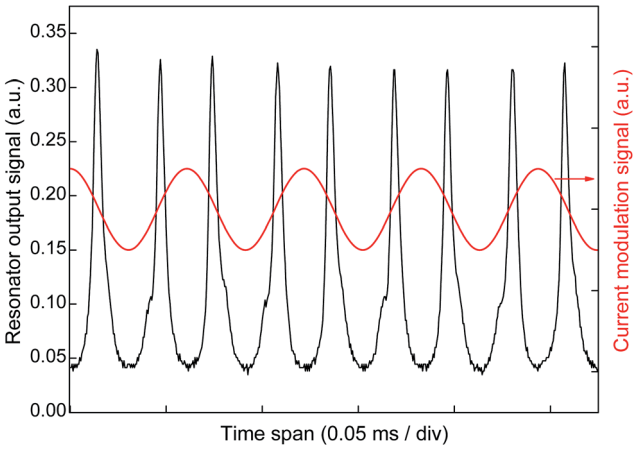

Fig. 3 The cavity output signal (black curve) under vacuum conditions, acquired by using the InSb detector in locking conditions when a 0.1 Hz tuning triangular ramp (not shown in the picture) and the sinusoidal modulation at 16 kHz (red curve) are applied to the QCL current driver.

0.1 Hz tuning triangular ramp (not shown in the picture) and the sinusoidal modulation at 16 kHz (red sinusoidal curve) are applied to the current driver.

The resonator output signal is not flat during the scan but it is characterized by a series of peaks at twice the frequency of the sinusoidal modulation. This behavior is expected if one considers that the PZT response is not fast enough to follow the fast dither at 16 kHz. Thus, the slow locking loop is able only to keep the optical cavity resonant with the laser frequency at the *center* of the fast dither during the slow tuning ramp. Consequently, the locking loop acts as a mechanical chopper at 32 kHz (f_0) for the infrared light radiation in the cavity, forcing the resonator to follow the slow tuning ramp but not the fast dither. The overall effect is to produce an amplitude modulation on the intracavity radiation interacting with the gas sample and leading to the generation of an acoustic wave at the QTF resonance frequency f_0.

I-QEPAS sensor validation

I-QEPAS spectral scans were realized by stabilizing the temperature of the QCL at 283 K while the laser frequency was linearly tuned across the selected molecular transition by applying a slow voltage ramp to the laser. In addition, a sinusoidal dither at $f_0/2$ was applied to the QCL as described above, both for locking the cavity and for generating the intracavity acoustic wave at the QTF resonance frequency f_0. Due to the "chopping" effect of the cavity, our sensor works in an amplitude modulation regime, and the I-QEPAS signal is obtained by demodulating the piezoelectric signal generated by the QTF at the same frequency f_0 with a lock-in amplifier.

To test our sensor we selected carbon dioxide (CO_2) as the target gas. CO_2 is the main product of combustion processes and human activities. Its monitoring has assumed primary importance for global control of the environment and for industrial, medical and geophysical purposes. We targeted the (00^01) – (00^00) P(42) roto-vibrational transition of CO_2 centered at 2311.105 cm^{-1} with a linestrength $S = 4.749 \times 10^{-19}$ cm mol^{-1} (HITRAN units). The selected line is free from interference of common air constituents (such as H_2O, CO, N_2O and CH_4).[24] We experimentally observed a strong absorption from ambient CO_2 in air, leading to a significant attenuation (~40% of the optical power at the center of the investigated line) of the laser beam along its open-air path (~30 cm) before entering the cavity. Therefore, starting from about 5.5 mW after the ZnSe collimating lens, the available power at the center of the absorption line was $P = 3$ mW before the input mirror, corresponding to an intracavity optical power of about $P_c = PE = 0.72$ W.

Working in the amplitude modulation regime, our sensor is affected by a non-negligible signal offset. The overall system response is the results of a sum of three components: (i) an unwanted background due to the acoustic signal, mostly due to the laser absorption by the windows; (ii) a contribution due to laser absorption by ambient CO_2 in the optical path outside the cavity; (iii) the I-QEPAS signal generated by the absorption of CO_2 in the pressure-controlled chamber. The background acoustic signal has a nearly wavelength-independent nature in the narrow spectral range corresponding to ~two times the CO_2 absorption linewidth, whereas the contribution to the absorption by ambient CO_2 in the air-path has a broad Lorentzian shape (when compared to the I-QEPAS signal), which can be estimated to have a 4.72 GHz full width at half maximum (FWHM). By acquiring background spectra with the optical cavity filled with pure nitrogen, we verified that the pure background signal can be fitted by a Lorentzian function (with the FWHM forced to the calculated value) plus a constant offset.[14] We consequently subtract the background components from all acquired spectra discussed in this work in order to extract the resulting I-QEPAS signal due to the gas sample filling the cavity.

In order to determine the best operating conditions, we studied the I-QEPAS signal dependence on the gas pressure and the laser modulation depth (induced by the sinusoidal dither). For this analysis a certified mixture of 860 parts-per-billion (ppb) of CO_2 in pure nitrogen (N_2) was used. In Fig. 4a is reported the I-QEPAS peak signal as a function of the laser modulation depth at a gas mixing pressure of 50 mbar. The peak signals were normalized to their maximum values. The results illustrate the influence of the laser modulation depth on the I-QEPAS signal. The region between 10 and 13 MHz appears quite flat, so we selected 10 MHz as the operating modulation depth. Using this modulation, we were able to completely scan the resonance of the cavity during each half period of the sinusoidal laser modulation. Fig. 4b depicts the I-QEPAS signal amplitude as a function of the sample pressure at 10 MHz modulation depth. The gas pressure influences the QEPAS signal mostly because the Q-factor decreases at higher pressures, while the vibrational–translational (V–T) energy transfer relaxation rate is faster at higher pressures, resulting in more efficient sound production. Therefore, there is a trade-off value for the pressure, where the I-QEPAS peak signal reaches its highest value. In our experiments, this condition is obtained for a gas pressure of 50 mbar.

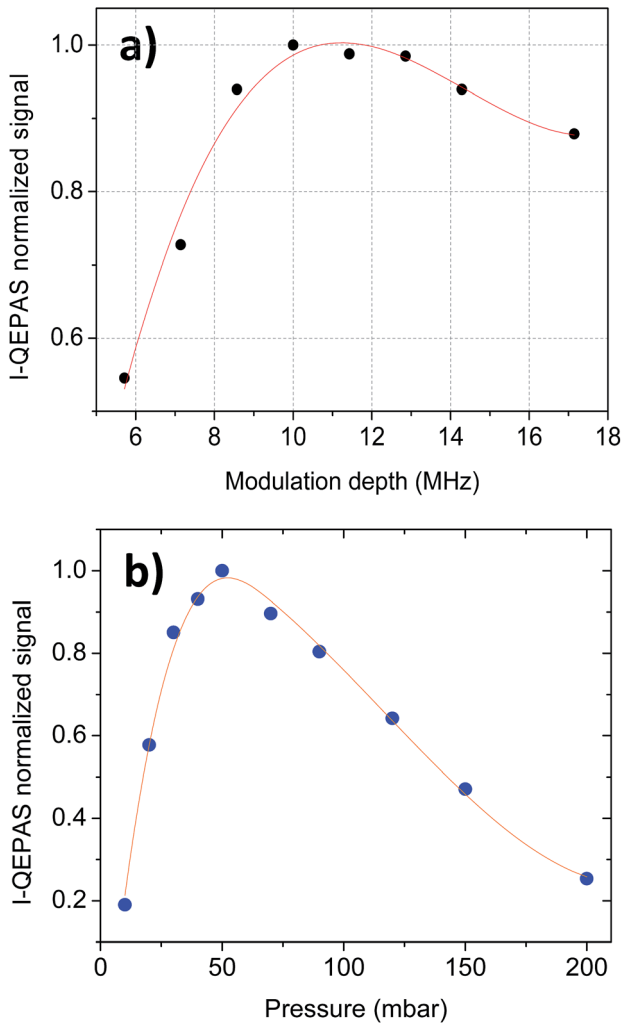

Fig. 4 (a) I-QEPAS signal amplitude plotted as a function of the modulation depth for a certified mixture of 860 ppb of CO_2 in pure N_2 at a total gas pressure of 50 mbar. The conversion factor between the modulation amplitude (peak-to-peak, in volts) and the laser frequency span is 140 MHz V^{-1}, obtained by previous calibration of the driver modulation input on the Doppler broadened molecular line. (b) I-QEPAS signal amplitude plotted as a function of total gas pressure with the same certified gas mixture and a modulation depth of 10 MHz. The solid line is a guide for the eye.

For the sensor validation, different CO_2 concentrations in the 860–50 ppb range were realized by diluting the calibration mixture of 860 ppb CO_2–N_2 in dry N_2. High-resolution I-QEPAS scans of CO_2–N_2 mixtures with 410 ppb, 300 ppb, 170 ppb, 90 ppb and 50 ppb CO_2 concentrations acquired with a lock-in time constant of 1 s are shown in Fig. 5. As expected I-QEPAS spectral scans do not show a 2nd derivative-like shape typical of $2f$ lock-in demodulation, but has a typical absorption-like profile of pure amplitude modulation detection. Considering the noise fluctuations of 3.5 mV (1σ value measured on the flat tails of the absorption lines) and the I-QEPAS peak signal of 170 mV at 50 ppb of CO_2 concentration, we can extract for our I-QEPAS sensor a 1σ detection limit of 1 ppb at 4 s averaging time.

The response of the sensor was investigated by plotting the I-QEPAS peak signal as a function of the CO_2 concentration

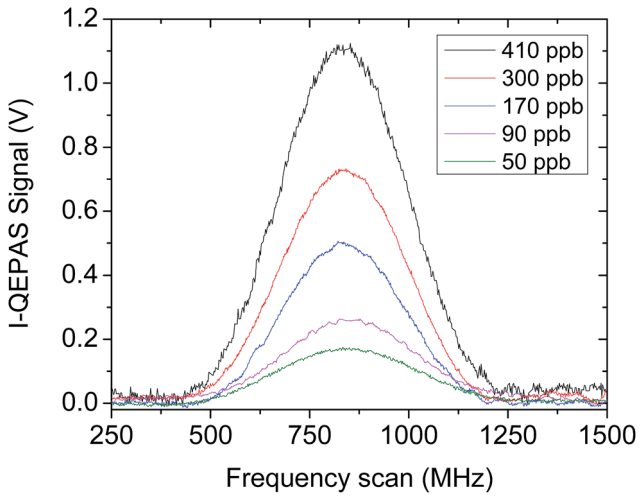

Fig. 5 I-QEPAS spectral scans of five representative CO_2 concentrations of 410 ppb, 300 ppb, 170 ppb, 90 ppb, and 50 ppb, obtained by diluting a certified mixture of 860 ppb of CO_2 in dry N_2. Scans are acquired with a modulation depth of 10 MHz, at a total gas pressure of 50 mbar and 4 seconds averaging time (1 s lock-in time constant).

between 0 ppb (pure N_2) and 860 ppb. High CO_2 concentrations induce absorption losses inside the cavity comparable with those due to the mirror leakage. This reduces the cavity finesse F, and thus both the power enhancement factor E and the intracavity optical power. Since the photoacoustic signal is directly proportional to the available optical power between the two prongs of the QTF, all the experimental data were normalized with a factor defined as $\rho = F/F_0$, where F_0 is the finesse of the resonator in a vacuum. This factor allows us to take into account the decreasing enhancement factor (and thus the intracavity power) with increasing internal absorption losses due to higher CO_2 concentrations, as shown in Fig. 6. Experimental data and normalized experimental data are also shown in Fig. 6.

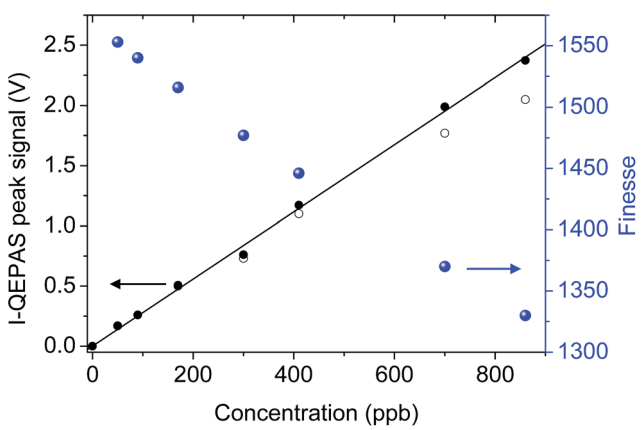

Fig. 6 Calculated cavity finesse values (●) plotted as a function of the concentrations of CO_2 in the compact vacuum chamber. As the concentration of CO_2 grows, the finesse falls down due to the increase of CO_2 absorption losses in the cavity. I-QEPAS signal amplitude (○ symbols) as a function of the CO_2 concentration, and actual I-QEPAS signal amplitude (● symbols) normalized taking into account the ρ factor. The solid line is the linear fit of the normalized QEPAS signals.

I-QEPAS peak signals attributed to low CO_2 concentrations (lower than 300 ppb) are not sensibly affected by the correction procedure confirming that our sensor works better at low gas target concentrations. For higher concentrations a standard QEPAS setup can be used or, alternatively, the correction procedure is mandatory.

Comparison with the standard QEPAS technique

In order to experimentally determine the enhancement in sensitivity induced by the optical power build-up approach, a set of measurements with the standard QEPAS approach was performed. The experimental setup is identical to that sketched in Fig. 1 except for the optical cavity that was removed. Now the collimated laser beam is focused directly between the prongs of the QTF. QEPAS spectral scans were performed by selecting the same absorption line and using a wavelength modulation (WM) approach and 2*f* detection: a sinusoidal dither at a frequency of $f_0/2$ was applied to the QCL through the FET controller and the QEPAS signal was demodulated at f_0 by means of a lock-in amplifier. The laser spectral scans are obtained by applying a slow voltage ramp to the current driver. The optimal sensor operating conditions were found to occur by working at a total gas pressure of 50 mbar and a modulation depth of 350 MHz. It worth noticing the strongly different modulation depths employed in QEPAS and I-QEPAS measurements. This is due to the different linewidths with which we have to deal in the two cases: the pressure-broadened molecular linewidth in QEPAS, the narrow width of the cavity mode in the I-QEPAS setup. We determined the QEPAS sensor baseline by acquiring a complete scan with the spectroscopic cell filled with pure N_2. We verified that in this case the spectroscopic signal had a flat zero background, as expected using the WM method. Different CO_2 concentrations in the 60–2.5 parts-per-million (ppm) range were generated by diluting a certified mixture of 100 ppm of CO_2 in N_2. Spectral scans of CO_2–N_2 mixtures with 56 ppm, 31 ppm and 11 ppm of CO_2 concentrations acquired with a lock-in time constant of 1 s are shown in Fig. 7.

Note that the QEPAS spectrum has a 2nd derivative lineshape as expected but is slightly distorted. This distortion is exhibited through an asymmetry on both sides of the spectrum around the peak position, and can be ascribed to a residual amplitude modulation contribution to a 2*f* detection approach.[25] The linearity of the QEPAS peak signal as a function of the gas concentration was investigated and the calibration curve, plotted in Fig. 8, was obtained.

In order to determine the best achievable sensitivity of both the QEPAS and I-QEPAS sensors we performed an Allan variance analysis measuring and averaging the signal at zero CO_2 concentration (pure N_2 in the chamber at 50 mbar) and with the laser frequency locked to the selected CO_2 absorption line. The comparison between the two Allan deviation plots is shown in Fig. 9. To verify the proportionality between the improvement in terms of sensitivity and the power enhancement factor we divided the QEPAS Allan plot by $E = 240$.

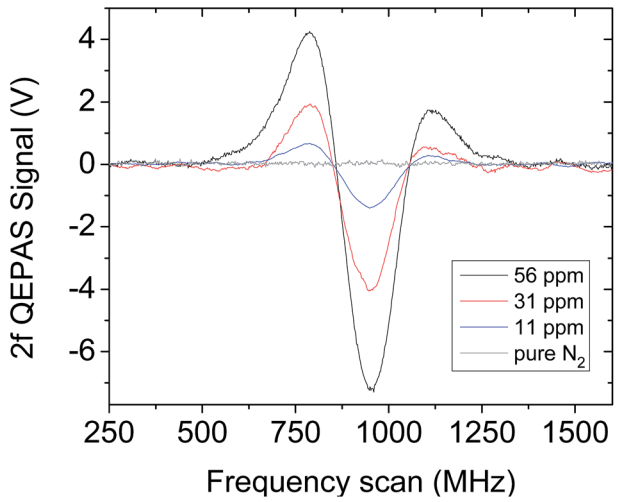

Fig. 7 QEPAS spectral scans of CO_2–N_2 mixtures with 56 ppm, 31 ppm and 11 ppm of CO_2 concentrations obtained by diluting a certified mixture of 100 ppm of CO_2 in dry N_2. A spectral scan obtained for pure N_2 is also shown. The operating conditions are: gas pressure of 50 mbar, modulation depth of 350 MHz and lock-in time constant of 1 s (4 s averaging time).

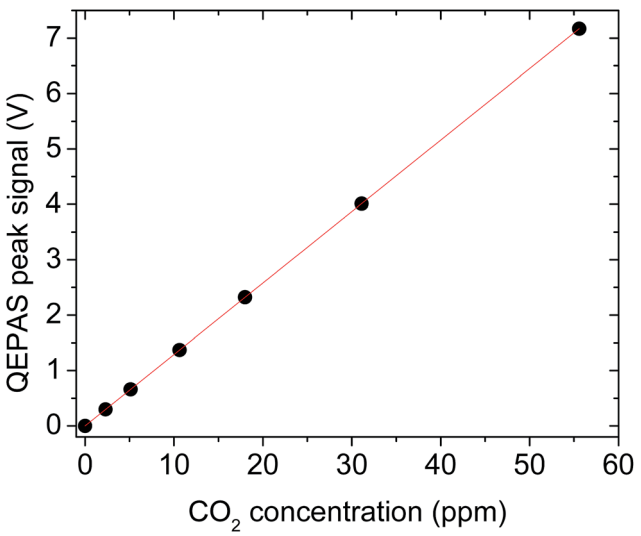

Fig. 8 QEPAS signal as a function of the CO_2 concentration. The solid line is the best linear fit of the experimental data. The linear correlation coefficient is $R = 0.0993$.

The comparison shows that after this rescaling the two curves almost overlap. The peaks (at ~8 s, 30 s and 50 s) in the I-QEPAS Allan deviation can be attributed to mechanical instabilities of the cavity and oscillations of the locking loop. The long term drift which marks the difference between the two curves from ~60 s on is probably due to thermal drifts of the cavity, which causes small fluctuations of the mirror positions and consequently of the beam waist. This produced a detectable effect on the QTF thermal noise. This effect can be canceled out by adopting proper temperature stabilization of the whole cavity, thus leading to improved sensitivities for longer

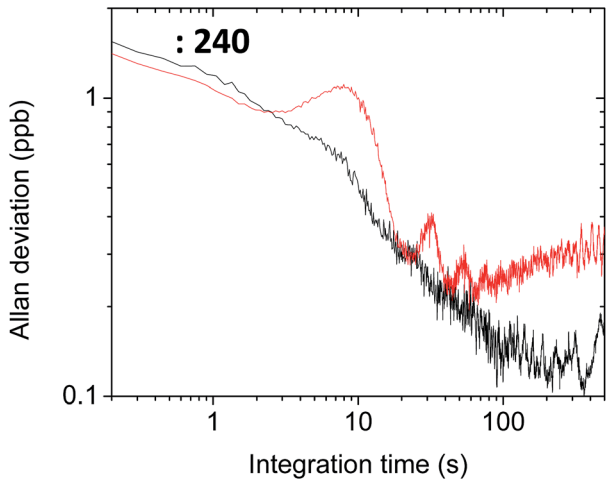

Fig. 9 Comparison between Allan deviation plots in ppb CO_2 concentrations, obtained for I-QEPAS (red curve), and standard QEPAS (black curve), as a function of the integration time. For the sake of comparison, the QEPAS Allan plot has been divided by the power enhancement factor $E = 240$.

integration times. For the QEPAS sensor at 20 s integration time we extract a 1σ minimum detectable concentration limit of 72 ppb, corresponding to $\alpha_{min} = 3.3 \times 10^{-6}$ cm^{-1} and a NNEA of 7.5×10^{-8} W cm^{-1} Hz$^{-1/2}$. At the same integration time, for the I-QEPAS sensor we estimated a 1σ equivalent concentration of 300 ppt, corresponding to a minimum absorption coefficient $\alpha_{min} = 1.4 \times 10^{-8}$ cm^{-1} and a normalized noise equivalent absorption (NNEA) of 3.2×10^{-10} W cm^{-1} Hz$^{-1/2}$. These results confirm the achievement of a sensitivity enhancement factor for the I-QEPAS sensor, with respect to the standard QEPAS, corresponding to the power enhancement factor.

Conclusions

The architecture and performance of a novel ultra-highly sensitive, selective and real-time gas sensor called I-QEPAS based on mid-IR QCL and QEPAS detection in an optical power buildup cavity were described. A continuous-wave 4.3 μm DFB QCL was used, allowing for about 3 mW optical power available at the input mirror of the cavity. A highly efficient injection of the QCL light into the cavity was achieved, leading to an intracavity laser power of ~0.7 W. The capability of automatically maintaining the cavity frequency locked to the laser frequency was demonstrated by means of a home-made built electronic circuit. A 1σ minimum detection limit of 300 ppt was achieved for an integration time of 20 s using an interference-free CO_2 absorption line, corresponding to a NNEA of 3.2×10^{-10} W cm^{-1} Hz$^{-1/2}$. The improvement in terms of sensitivity with respect to the conventional QEPAS setup (operating under the same conditions of molecular linewidth, pressure and laser output power) results to be equal to the power enhancement factor occurring in the optical resonator. This demonstrates the validity of our approach, which pushes I-QEPAS among the most sensitive cavity-based techniques as ICOS or CRDS when fast relaxing gases are used. Further improvements in sensitivity can in principle be achieved with resonators with higher finesse, provided that suitable narrow-linewidth radiation is available. Moreover, since a bare QTF was used as an acoustic detection module in our setup, further improvements are expected by adding metallic organ-pipe micro-resonators to the photoacoustic detection module. Finally, a breakthrough step will be replacing the PZT with a faster piezo actuator, able to follow the laser modulation at 16 kHz, so that it will be possible to implement a background-free WM I-QEPAS configuration.

Acknowledgements

This work was financially supported by the Italian Ministry for University and Research through the Italian national projects PON01_02238, PON02_00675, PON02_00576 and the project "Active Ageing@home"; within the National Technological Cluster (CTN) venture in the PON-2013-FESR framework.

Notes and references

1 M. Ebrahim-Zadeh and I. T. Sorokina, *Mid-Infrared Coherent Sources and Applications*, Springer, Houten, 2007.
2 M. Jahjah, W. Jiang, N. P. Sanchez, W. Ren, P. Patimisco, V. Spagnolo, S. C. Herndon, R. J. Griffin and F. K. Tittel, *Opt. Lett.*, 2014, **39**, 957–960.
3 S. Borri, S. Bartalini, P. De Natale, M. Inguscio, C. Gmachl, F. Capasso, D. L. Sivco and A. Y. Cho, *Appl. Phys. B*, 2006, **85**, 223–229.
4 G. Gagliardi and H. P. Loock, *Cavity-Enhanced Spectroscopy and Sensing*, Springer, London, 2014.
5 I. Galli, S. Bartalini, S. Borri, P. Cancio, D. Mazzotti, P. De Natale and G. Giusfredi, *Phys. Rev. Lett.*, 2011, **107**, 270802.
6 A. Elia, P. M. Lugarà, C. Di Franco and V. Spagnolo, *Sensors*, 2009, **9**, 9616–9628.
7 P. Patimisco, G. Scamarcio, F. K. Tittel and V. Spagnolo, *Sensors*, 2014, **14**, 6165–6206.
8 G. Wysocki, R. Lewicki, R. F. Curl, F. K. Tittel, L. Diehl, F. Capasso, M. Troccoli, G. Hofler, D. Bour, S. Corzine, R. Maulini, M. Giovannini and J. Faist, *Appl. Phys. B: Lasers Opt.*, 2008, **92**, 305–311.
9 A. A. Kosterev, Y. A. Bakhirkin, R. F. Curl and F. K. Tittel, *Opt. Lett.*, 2002, **27**, 1902–1904.
10 A. A. Kosterev, F. K. Tittel, D. Serebryakov, A. L. Malinovsky and I. Morozov, *Rev. Sci. Instrum.*, 2005, **76**, 1–9.
11 K. Liu, X. Guo, H. Yi, W. Chen, W. Zhang and X. Gao, *Opt. Lett.*, 2009, **34**, 1594.
12 V. Spagnolo, L. Dong, A. A. Kosterev and F. K. Tittel, *Opt. Express*, 2012, **20**, 3401–3407.
13 Y. Cao, W. Jin, L. H. Ho and Z. Liu, *Opt. Lett.*, 2012, **37**, 214–216.
14 V. Spagnolo, P. Patimisco, S. Borri, G. Scamarcio, B. E. Bernacki and J. Kriesel, *Opt. Lett.*, 2012, **37**, 4461–4463.
15 V. Spagnolo, P. Patimisco, S. Borri, G. Scamarcio, B. E. Bernacki and J. Kriesel, *Appl. Phys. B: Lasers Opt.*, 2013, **112**, 25–33.

16 Y. Ma, R. Lewicki, M. Razeghi and F. K. Tittel, *Opt. Express*, 2013, **21**, 1008–1019.
17 S. Borri, P. Patimisco, I. Galli, D. Mazzotti, G. Giusfredi, N. Akikusa, M. Yamanishi, G. Scamarcio, P. De Natale and V. Spagnolo, *Appl. Phys. Lett.*, 2014, **104**, 091114.
18 R. D. Van Zee and J. P. Looney, *Cavity-Enhanced Spectroscopies*, Academic Press, San Diego, 2002.
19 M. Hippler, C. Mohr, K. A. Keen and E. D. McNaghten, *J. Chem. Phys.*, 2010, **133**, 044308.
20 A. Kachanov, S. Koulikov and F. K. Tittel, *Appl. Phys. B: Lasers Opt.*, 2013, **110**, 47–56.
21 S. Bartalini, S. Borri, I. Galli, G. Giusfredi, D. Mazzotti, T. Edamura, N. Akikusa, M. Yamanishi and P. De Natale, *Opt. Express*, 2011, **19**, 17996–18003.
22 F. Cappelli, I. Galli, S. Borri, G. Giusfredi, P. Cancio, D. Mazzotti, A. Montori, N. Akikusa, M. Yamanishi, S. Bartalini and P. De Natale, *Opt. Lett.*, 2012, **37**, 4811–4813.
23 I. Galli, M. Siciliani de Cumis, F. Cappelli, S. Bartalini, D. Mazzotti, S. Borri, A. Montori, N. Akikusa, M. Yamanishi, G. Giusfredi, P. Cancio and P. De Natale, *Appl. Phys. Lett.*, 2013, **102**, 121117.
24 L. S. Rothman, I. E. Gordon, Y. Babikov, A. Barbe, D. Chris Benner, P. F. Bernath, M. Birk, L. Bizzocchi, V. Boudon, L. R. Brown, A. Campargue, K. Chance, E. A. Cohen, L. H. Coudert, V. M. Devi, B. J. Drouin, A. Fayt, J. M. Flaud, R. R. Gamache, J. J. Harrison, J. M. Hartmann, C. Hill, J. T. Hodges, D. Jacquemart, A. Jolly, J. Lamouroux, R. J. Le Roy, G. Li, D. A. Long, O. M. Lyulin, C. J. Mackie, S. T. Massie, S. Mikhailenko, H. S. P. Müller, O. V. Naumenko, A. V. Nikitin, J. Orphal, V. Perevalov, A. Perrin, E. R. Polovtseva, C. Richard, M. A. H. Smith, E. Starikova, K. Sung, S. Tashkun, J. Tennyson, G. C. Toon, V. G. Tyuterev and G. Wagner, *J. Quant. Spectrosc. Radiat. Transfer*, 2013, **130**, 4–50.
25 P. Patimisco, S. Borri, A. Sampaolo, H. E. Beere, D. A. Ritchie, M. S. Vitiello, G. Scamarcio and V. Spagnolo, *Analyst*, 2014, **139**, 2079–2087.